Overlap statistics of cumuliform boundary-layer cloud fields in large-eddy simulations

Roel A. J. Neggers,[1] Thijs Heus,[2] and A. Pier Siebesma[1,3]

R. A. J. Neggers, Royal Netherlands Meteorological Institute (KNMI), PO Box 201, 3730 AE De Bilt, The Netherlands. (e-mail: Roel.Neggers@knmi.nl)

[1]Royal Netherlands Meteorological Institute (KNMI)

[2]Max Planck Institüt für Meteorologie, Hamburg (MPI-M)

[3]Delft University of Technology, Delft, The Netherlands

Abstract. Overlap statistics of cumuliform boundary-layer clouds are studied using large-eddy simulations at high resolutions. The cloud overlap is found to be highly inefficient, due to the typical irregularity of cumuliform clouds over a wide range of scales. The detection of such inefficient overlap is enabled in this study by i) applying fine enough discretizations and ii) by limiting the analysis to exclusively cumuliform boundary-layer cloud fields. It is argued that these two factors explain the differences with some previous studies on cloud overlap. In contrast, good agreement exists with previously reported observations of cloud overlap as derived from lidar measurements of liquid water clouds at small cloud covers. Various candidate functional forms are fitted to the results, suggesting that an inverse linear function is most successful in reproducing the observed behavior. The sensitivity of cloud overlap to various aspects is assessed, reporting a minimal or non-systematic dependence on discretization and vertical wind-shear, as opposed to a strong case-dependence, the latter probably reflecting differences in the cloud size distribution. Finally, calculations with an offline radiation scheme suggest that accounting for the inefficient overlap in cumuliform cloud fields in a general circulation model can change the top-of-atmosphere short-wave cloud radiative forcing by -20 to -40 W m^{-2}, depending on vertical discretization. This corresponds to about 50 to 100 % of the typical values in areas of persistent shallow cumulus, respectively.

1. Introduction

Clouds significantly affect the earth's radiative budget, and the way clouds overlap in the vertical plays an important role in this process. A general circulation model (GCM) as used in the numerical prediction of weather and climate can not resolve cloud overlap within a vertical column, and accordingly it has to rely on parameterization. For these reasons the problem of cloud overlap has been actively researched in the last few decades [e.g. Geleyn and Hollingsworth, 1979; Barker, 2008]. While most studies of cloud overlap to date have concerned either the whole (i.e. troposphere-deep) atmosphere [e.g. Hogan and Illingworth , 2000] or deep convective clouds [Oreopoulos and Khairoutdinov, 2003; Pincus et al., 2005], the overlap in cumuliform boundary-layer cloud fields has recieved far less attention.

This study is exclusively concerned with vertical overlap in cumuliform boundary layer cloud fields. The scientific motivation for this choice is that the behavior of vertical overlap in this cloud regime is still relatively unknown. Cumuliform clouds are irregular in shape over a range of length-scales, due to their turbulent nature [e.g. Lovejoy, 1982; Cahalan and Joseph, 1989; Siebesma and Jonker, 2000]. The question how this cumuliform irregularity, especially at the smaller scales, influences the effective overlap is still unanswered. However, some evidence for inefficient overlap on small-scales does exist. Observational results were published by Brooks et al. [2004], who used surface lidar measurements and reported relatively inefficient overlap for liquid water clouds. Numerical evidence was published by Brown [1999], who used Large-Eddy Simulation (LES) at high vertical resolutions to find that overlap can be very inefficient in shallow cumulus cloud fields. While these reports of inefficient overlap in boundary-layer clouds already provide important insight into the problem and emphasize its relevance, what is still lacking is a more detailed analysis of this behavior over a range of depth-scales, from very small (∼ 1m) to typical GCM vertical grid-spacings (∼ 100m) and beyond (∼ 1000m).

A practical but important implication of the broad range of scales involved in cumuliform cloud overlap is that it could imply a problem in its parameterization for use in GCMs, as schematically illustrated in Fig. 1. At $10-50$ km the horizontal size of a **Fig. 1** present-day GCM gridbox is typically much larger than an individual shallow cumulus cloud; as a result, one GCM gridbox includes a whole ensemble of cumulus clouds. Given the small-scale irregularity of such cumulus cloud fields, both in the shape of individual clouds and in their spatial distribution, the vertical overlap will at least partially occur on depth-scales that are smaller than the vertical grid-spacings typical of present-day GCMs. This means that apart from a "super-grid scale" component, representing vertical overlap between model levels, a "sub-grid scale" (SGS) component is also required, representing the overlap on smaller scales. In principle all GCMs should account for the cloud overlap on subgrid-scales; however, to our knowledge no present-day operational GCMs does so. This means that the cloud fraction as produced by a parameterization and used for transport calculations might underestimate the cloud fraction appropriate for a radiation calculation [e.g. DelGenio et al., 1996; Brooks et al., 2004; Pincus et al., 2005]. This justifies further study of the vertical overlap in cloud regimes in which significant contributions by small-scale cloud structures can be expected.

This study aims to investigate more closely the impact of small-scale irregularity in cumuliform boundary layer cloud fields on the vertical overlap, again using LES as a research tool. We rely on the well-documented capacity of LES to resolve three-dimensional turbulence in an atmospheric domain at high resolutions, and to reproduce virtual but realistic cumulus cloud fields [e.g. Siebesma et al., 2003; Heus et al., 2010]. The specific questions addressed in this study are; i) how does overlap behave as a function of thickness of the layer of diagnosis, ii) how robust is this behavior, and iii) can it be captured by some functional relationship. To this purpose numerical simulations of various idealized cloudy boundary layer cases are performed. The sensitivity of the results to numerics as well as conditions will be assessed. The results will be discussed in the context of previous observational studies of cloud overlap. Finally, the impact of the cumuliform overlap found in this paper on radiative transfer will be explored through offline calculations with a GCM radiation scheme.

2. Diagnostics

The majority of previous studies on cloud overlap have relied on only two expressions. Both diagnostics will be calculated in this study; although the two expressions are not independent, in that they describe the same phenomenon, the main reason for including both is to allow the reader to put the results of this study in the context of previously published results. The exact definitions of both expressions, as applied in the discretized LES domain, are given in Appendix A. For simplicity only the short versions are given here.

2.1. Overlap ratio

The first expression for cloud overlap is that used by DelGenio et al. [1996] and Brooks et al. [2004], and relies on two different cloud fractions. It can be expressed as a 'cloud overlap ratio' r,

$$r = \frac{C_v}{C_p}, \tag{1}$$

where C_v is the cloud fraction "defined-by-volume", or the vertically averaged cloud fraction of layer Δ_z, and C_p is the cloud fraction "defined-by-area" (C_p), or the projected cloud cover over the layer. An attractive aspect of expression (1) is that C_v conceptually matches the cloud fraction as produced by one particular class of cloud schemes in GCMs, referred to as "statistical cloud schemes" [e.g. Mellor, 1977; Sommeria and Deardorff, 1977], that are based on assumed PDFs of total water. The inverse of ratio r can then be interpreted as the factor with which cloud fraction C_v should be multiplied to yield the projected cloud cover C_p as required by a radiative transfer scheme in a GCM.

2.2. Decorrelation length

The second method considers overlap between two LES model levels containing cloud as a function of their distance of separation Δz [Hogan and Illingworth , 2000]. The projected cloud cover is expressed as a linear interpolation between two theoretical limits of cloud overlap,

$$C_p = \alpha C_{max} + (1 - \alpha) C_{rand} \tag{2}$$

where C_{max} is the *maximum* overlap limit, or the hypothetical situation in which all cloudy layers perfectly overlap in the vertical, and C_{rand} is the *random* overlap limit, or the situation in which no correlation exists between the horizontal position of a cloud layer relative to its neighbour. Diagnosing C_p and calculating the maximum and random overlap limits then yields a value for α, the "overlap parameter". Hogan and Illingworth [2000] used cloud radar measurements to find that the dependence of α on layer separation follows an exponential,

$$\alpha = \exp\left(-\frac{\Delta z}{\Delta z_0}\right), \tag{3}$$

with Δz_0 the associated e-folding distance or "decorrelation length", its value ranging from 1.4 to 2.9 km depending on spatial and temporal discretization. Subsequent studies have found similar spread, documenting dependence on cloud regime [e.g. Oreopoulos and Khairoutdinov, 2003; Pincus et al., 2005].

3. Calculations

The LES calculations in this study are carried out using the Dutch Atmospheric Large-Eddy Simulation model [DALES, Heus et al., 2010]. Three different cumulus cases are simulated; the BOMEX case representing steady-state marine fair-weather cumulus [Siebesma et al., 2003], the ATEX case representing steady-state marine cumulus with capping outflow under a strong inversion [Stevens et al., 2001], and the ARM case representing transient continential cumulus at the Southern Great Plains (SGP) site on 21 June 1997 [Brown et al., 2002]. The BOMEX control experiment is vertically discretized at 10m. By default the simulated domain size is 6.4×6.4 km, except for the ARM case where a 25.6×25.6km domain was used to ensure statistical significance when diagnosing cloud overlap as a function of time. The cloud fields in all three cases can be described as fair-weather cumulus, as characterized by a relatively low total cloud cover ($10 - 20$ %) and a small domain average liquid water path ($5 - 10$ g m^{-2}). In the ATEX case however, the cumulus cloud field is topped by a capping outflow layer. Cloud base height is always at about $0.5 - 1$ km, and cloud top at about $1.5 - 2$ km. To give the reader an impression of a simulated cloud field, a snapshot of a BOMEX cloud field as generated by LES is shown in Fig. 2a. **Fig. 2**

For clarity we first study the impact of SGS overlap on cloud fraction in a single instantaneous three-dimensional cloud field from the BOMEX case. Figure 2b shows the profiles of C_p for various values of layer-depth Δz (as visualized in Fig. 1). At $\Delta z = 10$ m the layer-depth is equal to the vertical discretization in LES, which implies $C_p = C_v$. For increasing values of Δz, however, the projected cover C_p quickly increases relative to C_v, with an approximate doubling at $\Delta z = 200$ m and a quadrupling at $\Delta z = 600$ m. At $\Delta z = 1200$ m the layer-depth is approximately equal to the cloud-layer depth in BOMEX, and C_p is equal to the often-used "total cloud cover" as seen at the surface. Given the typical vertical grid-spacings of present-day GCMs at about $100 - 500$ m in the boundary layer, the impact of SGS overlap on cloud cover is significant. To improve the statistical significance the next step is to average over 60 instantaneous three-dimensional snapshots, each separated in time by 300s to ensure that the sampled cloud fields are independent. The time-averaging is achieved by accumulating the PDFs of all instantaneous snapshots. Figure 3a shows the results for the BOMEX case, now plotted as a **Figure 3** two-dimensional probability-density function (pdf) as a function of overlap ratio r and layer-depth Δz. The figure confirms that the vertical overlap in cumuliform boundary-layer cloud layers is very inefficient; the overlap ratio sharply reduces from 1 to about 0.4 over the first 200m.

The diagnosis of such inefficient cloud overlap in LES is not a novelty; various intercomparison studies of multiple LES codes for shallow cumulus convection have already established this behavior (see for example Siebesma et al. [2003], their Fig.2c and 6; and

Brown et al. [2002]). What is new in this study is i) the exploration of this behavior as a function of layer depth, and ii) viewing these results in the context of previous observational studies. First, due to the use of C_v and C_p the results shown in Fig. 3a can directly be compared to those reported by Brooks et al. [2004]. The inefficiency of the overlap found in this LES study agrees reasonably well with the lidar-derived overlap efficiency for liquid water clouds at small cloud cover as reported by Brooks et al. [2004]. Second, to allow comparison to the results of Hogan and Illingworth [2000], their decorrelation-length method is now applied to the LES fields, as shown in Fig. 3b. For reference their exponential fit with $\Delta z_0 = 1.6$ km is also shown. In LES the decay of α with separation distance Δz is much stronger, indicating much less efficient overlap. To quantify this behavior the e-folding depth Δz_0 is calculated over the lowest 300, yielding $\Delta z_0 = 220$ m. Also note that the pdf above 300m deviates from the exponential fit as applied to the lower part.

We speculate that various reasons can exist for the significant difference in cloud overlap efficiency as found in this study and as found by Hogan and Illingworth [2000]. First, the use of a different discretization (10m versus 300m vertical grid-spacing). Second, the application of a different sampling method (exclusively covering shallow cumulus clouds versus long-term coverage of the whole atmosphere, thus including clouds with much larger vertical extent). Third, the use of a different cloud detection criterion (non-zero condensate in LES gridboxes versus radar reflectivity). And finally, the cumulus cloud fields as simulated by LES might simply be unrealistic (although the good agreement with the observed overlap reported by Brooks et al. [2004], as well as the results of previous studies on cloud size statistics [e.g. Neggers et al., 2003] and cloud boundaries [e.g. Siebesma and Jonker, 2000] in LES, would suggest that this is not the case). Only the third option will be explored in this study; the others are for now regarded as future research topics.

4. Functional form

The next step is to establish which functional relationship best describes the shape of the overlap ratio pdf. More insight into functionality can be obtained by applying specific axis transformations to the plotting frame, by which certain functions will appear as a straight line. Least-square fitting the various candidate functions and comparing the associated root-mean-square errors (RMS) should then reveal which function is most successful. As candidate functions are considered those forms that have previously been applied in parameterizations of cloud overlap [DelGenio et al., 1996; Hogan and Illingworth , 2000; Brooks et al., 2004] or in describing cloud ensemble statistics[e.g. Plank, 1969; Cahalan and Joseph, 1989; Neggers et al., 2003], and include a power-law, an exponential and an inverse linear function.

Figure 4 shows three axis transformations as applied to the BOMEX pdf as shown in Fig. 3a. Table 1 documents the candidate functional forms and the results of their fit to the pdf. The log-log and log-linear transformations result in pdfs that still appear curved, and the associated powerlaw and exponential functions fail to satisfactorily capture the shape. In contrast, in the inverse linear transformation the pdf appears linear. Then comparing the root-mean-square values of the fit of each candidate function as given in Table 1 confirms that the inverse linear function $r = (1 + \beta \Delta z)^{-1}$ is most successful in capturing the shape of the pdf. The associated value of the constant of proportionality $\beta = 0.0064$ m^{-1} can be considered typical for the cloud overlap ratio in the BOMEX case.

Figure 4

Table 1

The question now arises what conceptual model can support the inverse linear function. This function implies that C_p grows with a constant value per height unit relative to C_v. Bodies like tilted Euclidian cylinders show this behavior, but not exclusively so; irregularly shaped bodies can behave similarly, for example when their axis follows a random-walk. More research is required to gain insight as to the appropriate conceptual model, both by looking at the overlap ratio of individual cumulus clouds and the impact of ensemble statistics.

5. Sensitivity

The inverse linear functional form is now used to explore the sensitivity of cloud overlap efficiency to resolution, domain-size, methodology and large-scale conditions. This is achieved by least-square fitting this function to the pdfs of various experiments and comparing the resulting values for the constant of proportionality β, as listed in Table 2. **Table 2**

The inefficient overlap at small depth-scales motivates the investigation of possible dependency on discretization in LES. We find a slight dependence on vertical resolution, with less efficient overlap at higher resolution; this might reflect the additional smaller clouds in the domain. A non-systematic variation is found for horizontal resolution, which is in contrast to the dependence found by Brown [1999]; a possible reason could be that the vertical resolution in our simulations (10 m) is much higher.

The cloud detection criterion as used in LES might affect the diagnosed cloud overlap statistics. It could also complicate the comparison to remote-sensing observations; instruments might in effect use a different criterion, and not 'see' very small condensate values, which could explain the more efficient overlap reported in some observational studies. For example, while lidars might be able to detect low values of liquid water, radars might not. To this purpose the sensitivity to the condensate-threshold $q_{c,crit}$ (as applied in the calculation of both c_k and I) is assessed. We find that the overlap efficiency is unaffected below $q_{c,crit} = 0.2$ g kg^{-1} and is actually *decreasing* above, probably reflecting that smaller but multiple parts of single whole clouds are then considered. Note that the above option would require an increasing overlap efficiency with condensate threshold; as we find the opposite dependence, this option can be excluded as a possible explanation for the less efficient overlap found in this study.

Brooks et al. [2004] proposed a power-law parameterization for the overlap ratio that also included a dependency on the horizontal grid-spacing in a GCM, reflecting the significant sensitivity to horizontal grid-spacing they observed for broken cloud fields ($0 < C_p < 1$). This would suggest that the LES results could depend on the domain-size of the LES simulation. To investigate, we repeated our analysis for a range of domain-sizes (3.2 - 25.6 km squared), with the largest size approaching the horizontal discretization of present-day operational GCMs. However, the overlap efficiency was not affected at all (not shown). One of the reasons for this insensitivity is probably the large number of cumulus clouds that are already present in the smallest domain-size. Another reason could be that the irregularity of individual clouds already constitutes much of the inefficient overlap as found for a whole cumulus ensemble. We further suspect that the broken cloud fields as sampled by Brooks et al. [2004] also include many cloud scenes that do not resemble the fair-weather cumulus cloud fields as exclusively investigated in this study (for example scenes with significant cloud cover).

Vertical wind-shear may tilt cumulus cloud and thus reduce overlap. This impact is investigated by comparing different experiments in which the wind shear over the cloud layer is 0x, 1x, 2x and 4x that of the control setup. Table 2 shows that a slight variation in β exists as a function of shear-intensity. This variation is much smaller than the absolute value in the no-shear experiment, in which the potential impact of Euclidian tilting is eliminated (i.e. all overlap is due to cloud irregularity). This suggests that the impact of small-scale cloud irregularity on overlap dominates over that of the Euclidian orientation of clouds.

Finally the case-dependence of cloud overlap ratio is explored. In the ARM case a clear diurnal cycle exists in the efficiency of cloud overlap, with a maximum in the late-afternoon. The probable reason is a shift in the cloud-size distribution, with the after-noon cumulus clouds being more shaped like well-defined towers, as opposed to the early and late hours of cloud existence when the cloud field consists of many small and shallow clouds. In this respect the ATEX case shows the same behavior; the cumulus outflow layer shows less efficient overlap compared to cumulus layer below, reflecting the existence of many small clouds at the evaporating edges of the cloud anvils (not shown). These results suggest that more information on the associated cloud size distributions is needed to understand the observed variation and to parameterize this behavior.

6. Impacts on radiative transfer

The results presented in the previous sections illustrate that SGS overlap significantly affects the projected cloud cover in cumuliform cloud fields. One then asks how this would affect the vertical transfer of radiation. While the subgrid-scale and grid-scale cloud overlap (or the 'inhomogeneity of cloud geometry') acts to increase the radiative impact of a given cloud field, at the same time the inhomogeneity of water content within the cloud field acts to reduce its radiative impact. These two different aspects of cloud inhomogeneity act as a pair of compensating effects; as of yet there has been insufficient information to effectively disentangle the two. However, as the fine discretizations as used in this LES study do give insight into one component of this compensating effect, namely the inhomogeneity of cloud geometry, it should now be possible to gain insight into the magnitude of the compensation. To this purpose an offline version of a radiation scheme of an operational GCM is fed with LES fields of the BOMEX case. We then compare the top-of-atmosphere (TOA) shortwave cloud radiative forcing, defined as the difference between the cloudy and clear-sky TOA net SW radiative flux, of calculations with and without representation of SGS overlap. In these experiments the inhomogeneity factor for water content as used in the radiation scheme is kept constant; the results will thus only reflect the impact of cloud geometry. Use is made of the radiation scheme of the ECMWF IFS Cycle 31r1 (Fouquart and Bonnel [1980]; Mlawer et al. [1997]; also described in great detail in the IFS CY31R1 documentation "Part IV: Physical processes", available on the internet at *http://www.ecmwf.int/research/ifsdocs/*). This code is used here as a representative of present-day numerical models for weather and climate prediction.

The calculations are set up as follows. To represent SGS overlap the inverse linear function (as defined in Table 1) is applied, using $\beta = 0.0064$ m^{-1} as obtained from the BOMEX case. For the super-grid scale overlap the radiation scheme by default applies the maximum-random overlap assumption; for the monotonically decreasing cloud fraction with height typical of shallow cumulus (see Fig. 2b) this assumption reverts to the maximum overlap function. To give the reader a sense of the dependency on cloud opacity the calculations are performed for a range of different cloud and condensate values; this is achieved by multiplying the BOMEX profiles of cloud fraction and condensate with a constant value, which preserves their vertical structure. Also, to illustrate dependency on vertical resolution, the radiation calculations are performed at two different discretizations, a fine one (L91) representing NWP models and a more coarse one representing climate models (L31). Both discretizations are visualized in Appendix B, showing that in the boundary layer the vertical grid-spacing in L31 is about twice that of L91.

In Fig. 5a and Fig. 5b the resulting change in the TOA SWCF is plotted as a function of liquid water path and maximum cloud fraction. Note that the spatial structure of this map should be interpreted as a 'fingerprint' of the IFS radiation scheme, and might differ for different codes. Individual points representing some shallow cumulus cases are included, for reference. The SGS overlap always makes the cloud layer less transparent in the short-wave; the change in TOA SWCF depends on the opacity of the cloud field, and ranges between cases from -5 W m^{-2} (BOMEX) to -17 W m^{-2} (ATEX) for L91. At the more coarse L31 discretization the impact is about twice as large. These numbers are put into better perspective by normalizing the field with the TOA SWCF of the no-SGS-overlap experiment, as plotted in Fig. 5c and Fig. 5d, giving the relative change that is introduced by including SGS overlap. The relative change is always substantial, at about $40-50$ % for L91 and $80-100$ % for L31. In areas of persistent shallow cumulus, such as in the marine subtropics, the representation SGS cloud overlap will thus significantly modify the radiative budget in a GCM. **Fig. 5**

When interpreting these changes in radiative flux it is important to keep in mind that they only reflect one component of a pair of compensating effects; the question how the inhomogeneity factor for water content changes is still unanswered, and requires further research. An LES model with an interactive radiation scheme could be used to answer this question.

7. Conclusions

This study uses LES to explore overlap in cumuliform boundary-layer cloud fields, and suggests a general functional relationship to describe this behavior. The cloud overlap is found to be highly inefficient, due to the typical irregularity of cumuliform clouds over a wide range of scales. Good agreement is reported with previously reported lidar-derived overlap for liquid water clouds at low cloud cover. The statistical reason for the difference with some other observational studies is twofold, namely i) differences in discretization of the analysis and ii) differences in sampling. Considerable spread is found in cloud overlap efficiency over various cases, probably reflecting differences in the cloud size distribution.

The inefficient overlap in cumuliform boundary-layer cloud fields as found in this study has implications for associated parameterizations in GCMs. In case GCM cloud schemes are configured to produce a volume-averaged cloud fraction (C_v), such as is the case with statistical cloud schemes, then the accompanying cloud overlap function should reproduce the inefficient overlap as observed in this study when applied to cumuliform boundary-layer cloud layers, both on supergrid-scale and subgrid-scale. If not, the effective cloud-radiative model climate will be complicated, as illustrated by the offline calculations with a GCM radiation scheme. In areas of persistent shallow cumulus, the radiative bias introduced by not accounting for SGS overlap can be as large as half the SWCF at typical NWP resolutions, and as large as the whole SWCF at typical climate model resolutions.

The results obtained in this study raise some new questions. Most important perhaps is to obtain further observational evidence to support the presented LES results, requiring high-frequency measurements of the three-dimensional structure of cumuliform cloud fields. This would require simultaneous measurement from different angles, due to the typical high opacity of individual cumuliform boundary-layer clouds. The recently-developed technique of 'volume scanning' by multiple radars or lidars could perhaps be used to this purpose. A fair comparison with this study also requires time-averaging over exclusively cumuliform boundary-layer days. A second open question raised by this study is the precise role of cloud ensemble statistics versus that of individual cumulus clouds in establishing the inefficient overlap, the associated functional form, and the case-dependence of its constant of proportionality. These topics are subject to ongoing research by the authors.

Appendix A: Overlap expressions

A1. Overlap ratio

Consider a layer of air in the LES domain of a certain thickness Δz that is situated within the cumulus cloud layer and that spans a number of LES model levels (as illustrated in Fig. 1). Suppose the LES-levels at the bottom and top of the layer are labeled k_0 and k_1, respectively, and that c_k is the cloud fraction at LES-level k. We now follow Brooks et al. [2004] by defining two different cloud fractions for this layer. The first is the cloud fraction "defined-by-volume" (C_v), or the vertically averaged cloud fraction of the layer,

$$C_v{}^{k_0,k_1} = \frac{1}{k_1 - k_0 + 1} \sum_{k=k_0}^{k_1} c_k, \tag{A1}$$

The second is the cloud fraction "defined-by-area" (C_p), or the projected cloud cover over the layer,

$$C_p{}^{k_0,k_1} = \frac{1}{i_{max} j_{max}} \sum_{i=1}^{i_{max}} \sum_{j=1}^{j_{max}} I^{k_0,k_1}(i,j), \tag{A2}$$

where i and j are the horizontal grid-indices, and I is a function which expresses the presence of condensate in the column between level k_0 and k_1 at coordinates i and j. Taking the ratio of (A1) to (A2) then yields an expression for the effective cloud overlap in the layer,

$$r^{k_0,k_1} = \frac{{C_v}^{k_0,k_1}}{{C_p}^{k_0,k_1}}, \tag{A3}$$

a ratio that is always smaller than one. The behavior of the overlap ratio as a function of layer depth Δz is studied by taking an instantaneous three-dimensional field of condensate $q_c(i,j,k)$ from LES and calculating ratio r^{k_0,k_1} for all possible combinations of k_0 and k_1 for which $k_1 \geq k_0$ and for which the model levels included in the layer all have $c_k > 0$. In other words, $r(\Delta z)$ will represent the overlap ratio of all sets of adjacent cloudy LES levels which span thickness Δz and which can be situated anywhere between the lowest cloud base and the highest cloud top in LES.

A2. Decorrelation length

The second method considers overlap between two LES model levels containing cloud as a function of their distance of separation [Hogan and Illingworth , 2000]. The projected cloud cover is expressed as a linear interpolation between two theoretical limits of cloud overlap,

$$C_{true} = \alpha C_{max} + (1-\alpha) C_{rand} \tag{A4}$$

where C_{max} is the *maximum* overlap limit,

$$C_{max} = \max\left(c_{k_0}, c_{k_1}\right) \tag{A5}$$

and C_{rand} is the *random* overlap limit,

$$C_{rand} = c_{k_0} + c_{k_1} - c_{k_0} c_{k_1}. \tag{A6}$$

Appendix B: IFS vertical discretizations

The 31-level (L31) and the operational 91-level (L91) vertical discretizations of the Integrated Forecasting System (IFS) of the European Centre for Medium-range Weather Forecasts (ECMWF) are plotted in Fig. 6. **Fig. 6**

Acknowledgments. We thank Robin Hogan, Anthony Illingworth, Gerd-Jan van Zadelhoff and Thorsten Mauritsen for their valuable feedback on preliminary results, and for recommending relevant literature on cloud overlap. We furthermore thank Malcolm Brooks and two anonymous reviewers for their knowledgeable and constructive comments on this manuscript.

References

Barker, H. W., 2008: Representing cloud overlap with an effective decorrelation length: An assessment using Cloudsat and CALIPSO data. *J. Geophys. Res.*, **113**, D24205, DOI:10.1029/2008JD010391.

Brooks, M. E., R. J. Hogan, and A. J. Illingworth, 2004: Parameterizing the difference in cloud fraction defined by area and by volume as observed with radar and lidar. *J. Atmos. Sci.*, **62**, 2248-2260.

Brown, A. R., 1999: Large-eddy simulation and parameterization of the effects of shear on shallow cumulus convection. *Bound. Lay. Meteor.*, **91**, 65-80.

Brown, A. R., and Co-authors, 2002: Large-eddy simulation of the diurnal cycle of shallow cumulus convection over land. *Quart. J. Roy. Met. Soc.*, **128**, 1075-1094.

Cahalan, R. F., and J. H. Joseph, 1989: Fractal statistics of cloud fields. *Mon. Wea. Rev.*, **117**, 262-271.

Del Genio, A. D., M.-S. Yao, W. Kovari, and K. K. Lo, 1996: A prognostic cloud water parameterization for global climate models. *J. Climate*, **9**, 270-304.

Fouquart, Y. and Bonnel, B., 1980: Computations of solar heating of the earth's atmosphere: A new parameterization. *Beitr. Phys. Atmos.*, **53**, 35-62.

Geleyn, J. F., and A. Hollingsworth, 1979: An economical analytical method for the computation of the interaction between scattering and line absorption of radiation. *Contrib. Atmos. Phys.*, **52**, 1-16.

Heus, T., and Co-authors, 2010: Formulation of the Dutch Atmospheric Large-Eddy Simulation (DALES) and overview of its applications *Geosci. Model. Dev.*, **3**, 415-444, DOI:10.5194/gmd-3-415-2010.

Hogan, R. J., and A. J. Illingworth, 2000: Deriving cloud overlap statistics from radar. *Quart. J. R. Meteorol. Soc.*, **126**, 2903-2909.

Hogan, R. J., and A. J. Illingworth, 2003: Parameterizing ice cloud inhomogeneity and the overlap of inhomogeneities using cloud radar data. *J. Atmos. Sci.*, **60**, 756-767.

Lovejoy, S., 1982: Area-perimeter relation for rain and cloud areas. *Science*, **216**, 185-187.

Mellor, G. L., 1977: The Gaussian cloud model relations. *J. Atmos. Sci.*, **34**, 356-358.

Mlawer, E. J., Taubman, S. J., Brown, P. D., Iacono, M. J. and CLough, S. A., 1997: Radiative transfer for inhomogeneous atmospheres: RRTM, a validated correlated-k model for the longwave. *J. Geophys. Res.*, **102D**, 16663-16682.

Neggers, R. A. J., H. J. J. Jonker, A. P. Siebesma, 2003: Size statistics of cumulus cloud populations in large-eddy simulation. *J. Atmos. Sci.*, **60**, 1060-1074.

Oreopoulos, and M. Khairoutdinov, 2003: Overlap properties of clouds generated by a cloud-resolving model. *J. Geophys. Res.*, **108**, D15, 4479, DOI:10.1029/2002JD003329.

Plank, V. G., 1969: The size distributions of cumulus clouds in representative Florida populations. *J. App. Met.*, **8**, 46-67.

Pincus, R., C. Hannay, S. A. Klein, K.-M. Xu, and R. Hemler, 2005: Overlap assumptions for assumed probability distribution function cloud schemes in large-scale models. *J. Geophys. Res.*, **110**, D15S09, DOI:10.1029/2004JD005100.

Siebesma, A. P., and H. J. J. Jonker, 2000: Anomalous scaling of cumulus cloud boundaries. *Phys. Rev. Lett.*, **85**, 214-217. DOI:10.1103/PhysRevLett.85.214

Siebesma, A. P., and Co-authors, 2003: A large eddy simulation intercomparison study of shallow cumulus convection. *J. Atmos.Sci.*, **60**, 1201-1219.

Sommeria, G., and J. W. Deardorff, 1977: Subgrid-scale condensation in models of non-precipitating clouds. *J. Atmos. Sci.*, **34**, 344-355.

Stevens, B., and Co-authors, 2001: Simulations of Trade-wind cumuli under a strong inversion. *J. Atmos. Sci.*, **58**, 1870-1891.

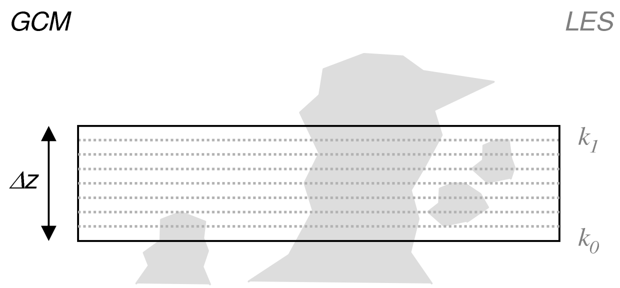

Figure 1. Schematic illustration of a GCM model level with thickness Δz that is situated inside a cloud layer containing irregular cumuliform boundary-layer clouds. The much finer LES discretization is visualized as dotted grey lines, with k_0 and k_1 being the LES levels at the bottom and top of the GCM layer, respectively.

a)

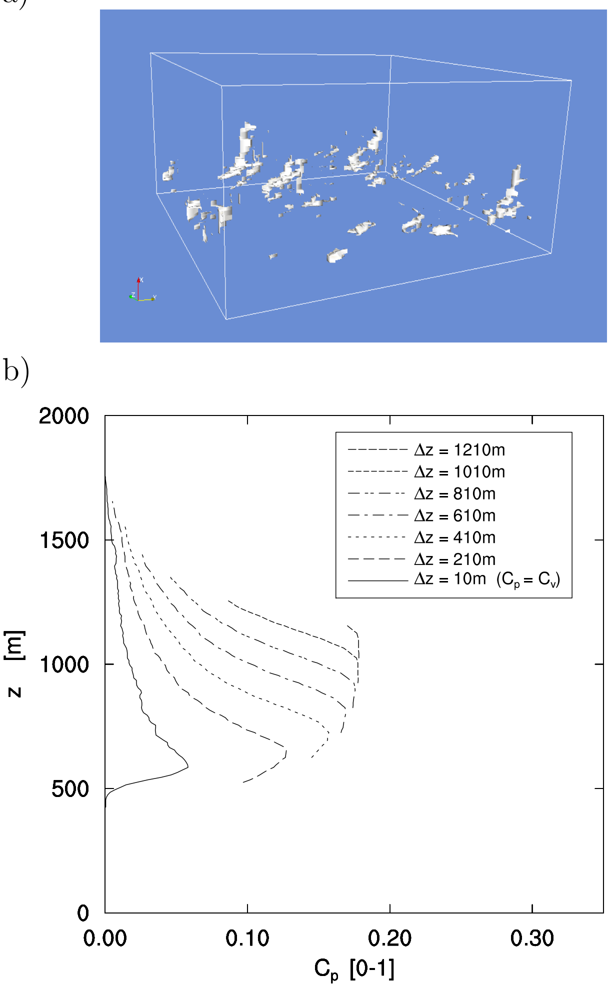

Figure 2. a) A snapshot of an instantaneous 3D cloud field during BOMEX as generated by LES. The domain size is 6.4 × 6.4 km. b) Profiles of C_p as a function of Δz for the snapshot shown in a).

a) b)

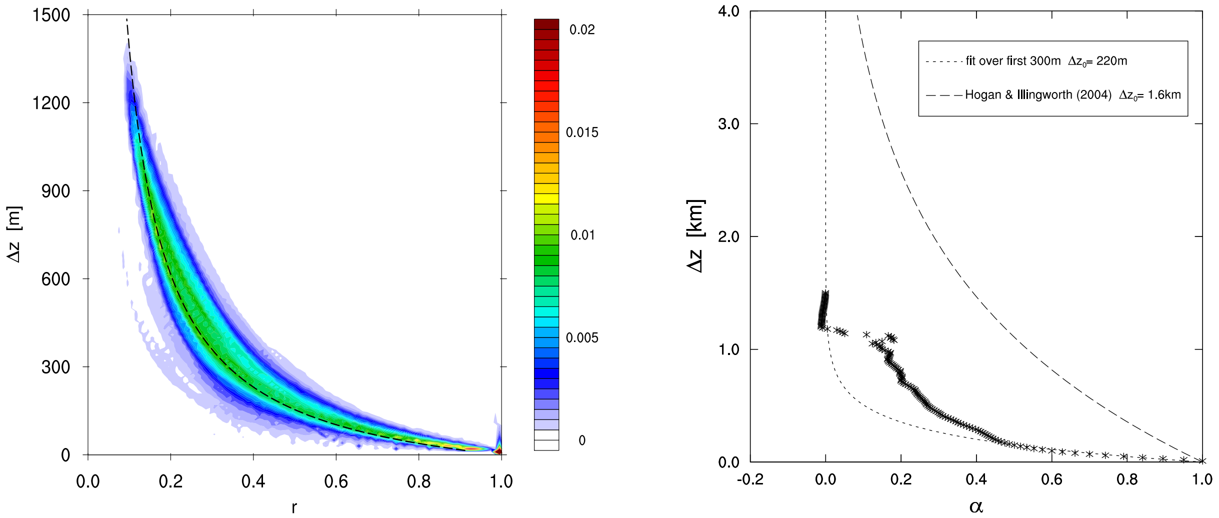

Figure 3. Two visualizations of overlap statistics for the BOMEX case. a) The probability density function P of the cloud overlap ratio r as a function of the layer thickness Δz. The contoured field represents $P \Delta h^{-1} \Delta r^{-1}$, with $\Delta r = 0.01$ and $\Delta h = 10$ m the respective binning-sizes on the r and Δz axes that were used to create the PDF. The dashed line represents the least-squares fit of the function $r = (1+\beta \Delta z)^{-1}$, as discussed in Section 4. b) The overlap parameter α as a function of separation distance Δz (asterisks). The dashed line represents the exponential fit of Hogan and Illingworth [2000], while the dotted line represents the exponential fit through the lowest 300 m of the LES data.

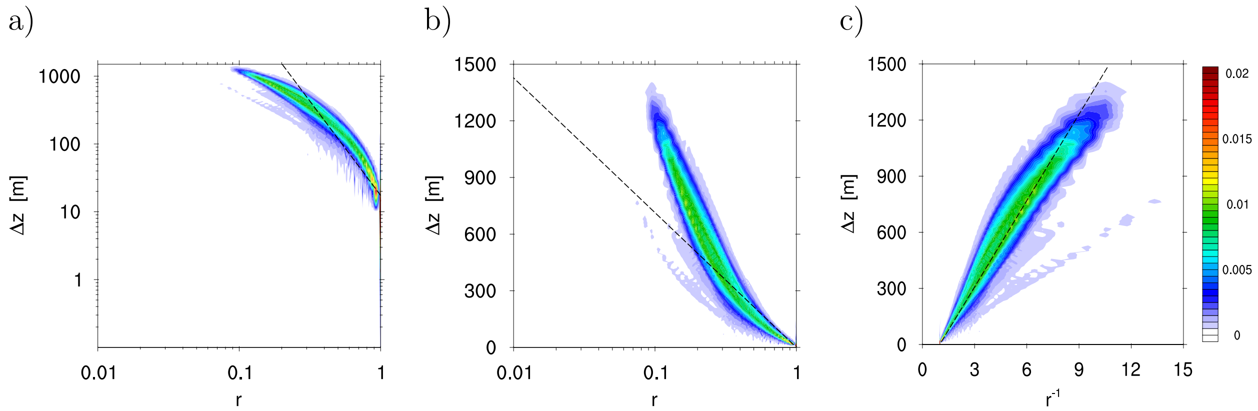

Figure 4. Same pdf as shown in Fig.3a, but now plotted using three different axis-transformations; a) log-log, b) log-linear, and c) using r^{-1} instead of r. The straight dashed line represents the least-square fit of a) a powerlaw function, b) an exponential function and c) an inverse linear function, respectively. These functions and the associated constants of proportionality are given in Table 1.

Table 1. Candidate Functional Forms[a]

Name	Function	Constants	RMS
Exponential	$r = \exp\left(-\frac{\Delta z}{\Delta z_0}\right)$	$\Delta z_0 = 310$ m	0.10105
Powerlaw	$r = a\Delta z^b$	$a = 2.8$	0.08053
		$b = -0.36$	
Inverse linear	$r = \frac{1}{1+\beta\Delta z}$	$\beta = 0.0064$ m^{-1}	0.04229

[a] The functional forms are fitted to the pdf as shown in Fig. 4. Columns 3 and 4 give the associated constants of proportionality and the root-mean-square error in r, respectively.

Table 2. Cloud Overlap Sensitivity

BOMEX vertical grid-spacing	β
10 m control	0.0064
20 m	0.0057
40 m	0.0051
BOMEX horizontal grid-spacing	β
100 m control	0.0064
50 m	0.0059
25 m	0.0065
BOMEX cloud criterion	β
$q_c > 0$ g kg^{-1} control	0.0064
$q_c > 0.1$ g kg^{-1}	0.0064
$q_c > 0.2$ g kg^{-1}	0.0073
$q_c > 0.5$ g kg^{-1}	0.0116
BOMEX wind shear	β
0x	0.0057
1x control	0.0064
2x	0.0064
4x	0.0066
ARM SGP local time	β
08:30	0.0480
09:30	0.0263
10:30	0.0137
11:30	0.0080
12:30	0.0054
13:30	0.0044
14:30	0.0041
15:30	0.0039
16:30	0.0039
17:30	0.0048
18:30	0.0065
19:30	0.0203
ATEX sampling height-range	β
Whole cloud layer	0.0097
Capping outflow layer (1200-2000m)	0.0133
Remainder (0-1200m)	0.0088

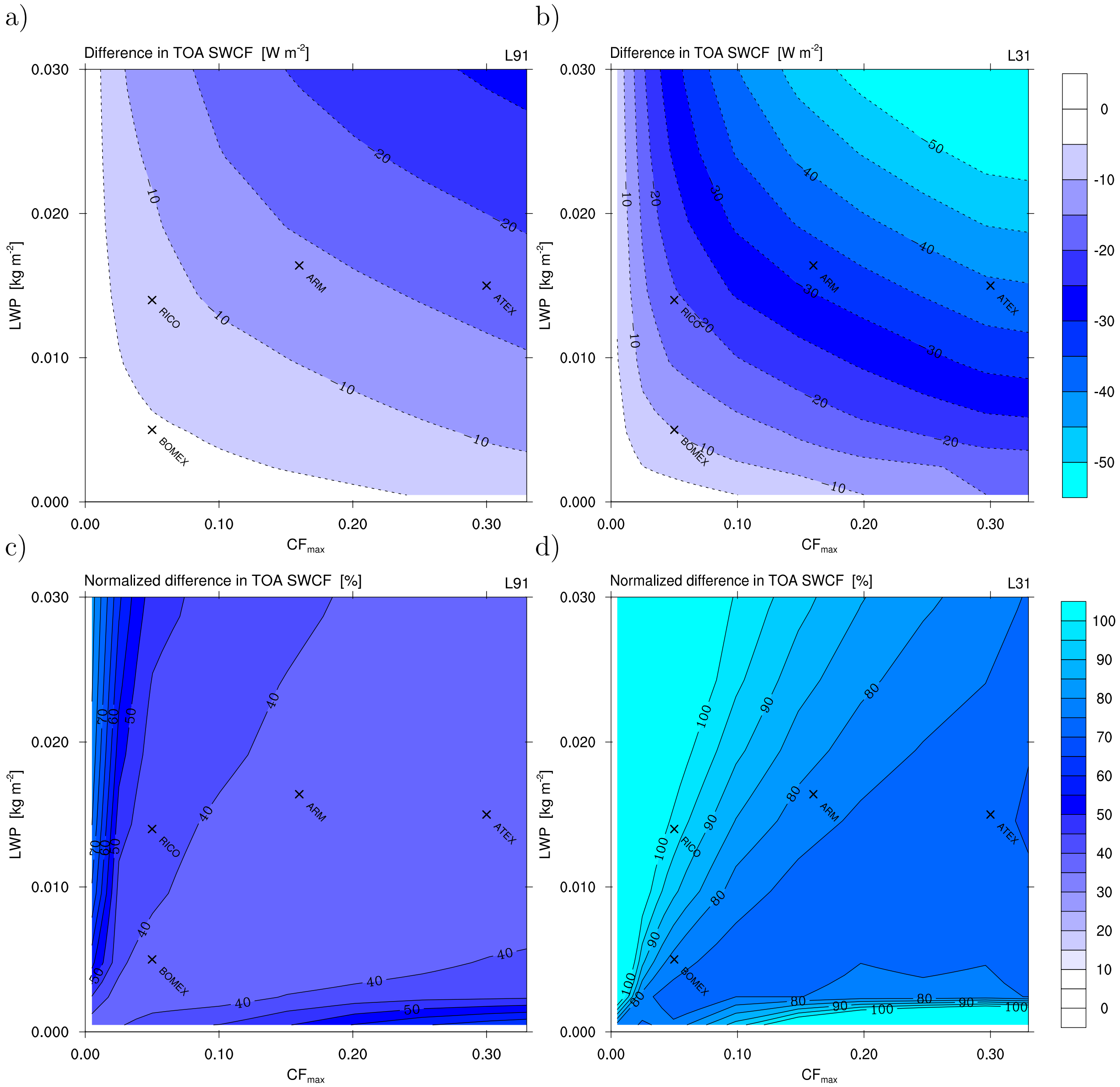

Figure 5. Impact of SGS overlap on the short-wave cloud-radiative forcing (SWCF) at the top of the atmosphere, plotted as a function of liquid water path (LWP) and maximum cloud fraction (CF_{max}). Use is made of the IFS radiation scheme, fed with profiles of cloud fraction and condensate as obtained from LES BOMEX. Plotted is the difference in TOA SWCF between a calculation with and without SGS overlap, for the vertical resolutions a) L91 (fine) and b) L31 (coarse). Panels c) and d) show the percentage change in the L91 and L31 TOA SWCF relative to the TOA SWCF of the calculation without SGS overlap. The properties of various shallow cumulus cases are indicated, for reference.

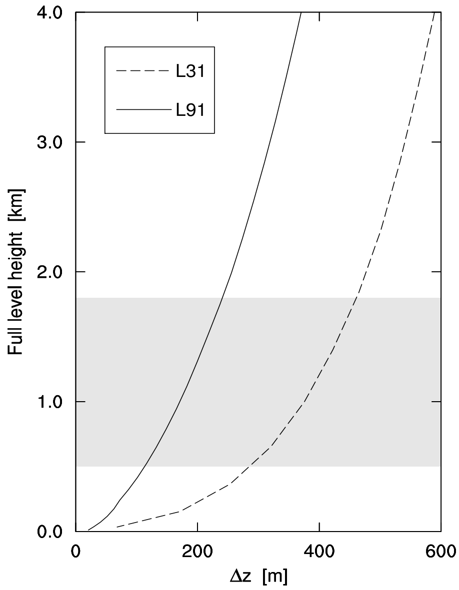

Figure 6. The L31 and L91 vertical discretizations of the ECMWF IFS as used in the radiation calculations. Plotted is the full-level thickness Δz as a function of full-level height, within the lowest 4 km. For reference the location of the cloud layer in the BOMEX case is indicated by the grey shading.

Figure Captions

Figure 1. Schematic illustration of a GCM model level with thickness Δz that is situated inside a cloud layer containing irregular cumuliform boundary-layer clouds. The much finer LES discretization is visualized as dotted grey lines, with k_0 and k_1 being the LES levels at the bottom and top of the GCM layer, respectively.

Figure 2. a) A snapshot of an instantaneous 3D cloud field during BOMEX as generated by LES. The domain size is 6.4×6.4 km. b) Profiles of C_p as a function of Δz for the snapshot shown in a).

Figure 3. Two visualizations of overlap statistics for the BOMEX case. a) The probability density function P of the cloud overlap ratio r as a function of the layer thickness Δz. The contoured field represents $P\Delta h^{-1}\Delta r^{-1}$, with $\Delta r = 0.01$ and $\Delta h = 10$ m the respective binning-sizes on the r and Δz axes that were used to create the PDF. The dashed line represents the least-squares fit of the function $r = (1 + \beta\Delta z)^{-1}$, as discussed in Section 4. b) The overlap parameter α as a function of separation distance Δz (asterisks). The dashed line represents the exponential fit of Hogan and Illingworth [2000], while the dotted line represents the exponential fit through the lowest 300 m of the LES data.

Figure 4. Same pdf as shown in Fig.3a, but now plotted using three different axis-transformations; a) log-log, b) log-linear, and c) using r^{-1} instead of r. The straight dashed line represents the least-square fit of a) a powerlaw function, b) an exponential function and c) an inverse linear function, respectively. These functions and the associated constants of proportionality are given in Table 1.

Figure 5. Impact of SGS overlap on the short-wave cloud-radiative forcing (SWCF) at the top of the atmosphere, plotted as a function of liquid water path (LWP) and maximum cloud fraction (CF_{max}). Use is made of the IFS radiation scheme, fed with profiles of cloud fraction and condensate as obtained from LES BOMEX. Plotted is the difference in TOA SWCF between a calculation with and without SGS overlap, for the vertical resolutions a) L91 (fine) and b) L31 (coarse). Panels c) and d) show the percentage change in the L91 and L31 TOA SWCF relative to the TOA SWCF of the calculation without SGS overlap. The properties of various shallow cumulus cases are indicated, for reference.

Figure 6. The L31 and L91 vertical discretizations of the ECMWF IFS as used in the radiation calculations. Plotted is the full-level thickness Δz as a function of full-level height, within the lowest 4 km. For reference the location of the cloud layer in the BOMEX case is indicated by the grey shading.